

Supporting Information:

Wetting Behavior of Polyelectrolyte Complex Coacervates on Solid Surfaces

Christopher Balzer,^{*,†} Pengfei Zhang,[‡] and Zhen-Gang Wang^{*,†}

*†Division of Chemistry and Chemical Engineering, California Institute of Technology,
Pasadena, California 91125, United States*

*‡State Key Laboratory for Modification of Chemical Fibers and Polymer Materials, Center
for Advanced Low-Dimension Materials, College of Material Science and Engineering,
Donghua University, Shanghai 201620, China*

E-mail: balzer@caltech.edu; zgw@caltech.edu

Contents

List of Figures	S-2
S1 Numerics of Turning Points	S-3
S2 Thermodynamic Stability and Turning Points	S-4
S3 First to Second Order Surface Transition	S-6
S4 Symmetric Adsorption with Applied Potential	S-7
S5 Interfacial Tension in Contact Angle Calculation	S-8
S6 Additional Prewetting Transition (Layering Transition)	S-9
S7 Effect of Polyelectrolyte Adsorption on Supernatant Surface Tension	S-10
References	S-11

List of Figures

S1	Graphical illustration of pseudo-arclength continuation	S-4
S2	Example adsorption isotherm and surface tension for first order transition . .	S-5
S3	Surface tension for adsorption isotherm below wetting point	S-6
S4	Surface free energy diagram for asymmetric adsorption	S-6
S5	Interfacial profiles for an applied potential	S-7
S6	Interfacial tension as a function of salt concentration	S-8
S7	Prewetting transition induced by applied potential	S-9
S8	Comparison of supernatant descriptions - Surface tension	S-10
S9	Comparison of supernatant descriptions - Contact angle	S-11

S1 Numerics of Turning Points

Computing the adsorption isotherms with a first order surface transition cannot be done via natural parameter continuation of the bulk polyelectrolyte density due to the presence of turning points. To overcome this, we use pseudo-arclength continuation (PAC)^{S1,S2} to vary the bulk polyelectrolyte density when computing adsorption isotherms. Such an approach is commonly used to study wetting.^{S3-S6} We will highlight the differences in our approach compared to the usual PAC.

Consider the nonlinear system $\mathbf{F}(\mathbf{X}; \lambda) = 0$, where \mathbf{X} can be thought of as the discretized density and electrostatic potential fields, $\mathbf{F}(\mathbf{X}; \lambda)$ are the corresponding mean-field equations, and λ is a continuation parameter, such as the bulk polyelectrolyte density. For a given value of λ , one can solve the equation $\mathbf{F}(\mathbf{X}; \lambda) = 0$. Natural continuation of λ would proceed by starting with λ_0 and taking steps in $\Delta\lambda$. However, if there are turning points in $\|\mathbf{X}\|$ versus λ , corresponding to singular points, natural continuation will fail.^{S7} To address this, we can instead solve the extended system $G = [\mathbf{F}(\mathbf{X}(s), \lambda(s)), N(\mathbf{X}(s), \lambda(s))]$ where λ is now undetermined and \mathbf{X} and λ are parameterized over an arclength variable s . Instead of taking steps of $\Delta\lambda$, one takes steps of the arclength variable of size Δs . The extended system requires specifying a new equation related to the arclength step, $N(\mathbf{X}(s), \lambda(s)) = \dot{\mathbf{x}}_0 \cdot (\mathbf{X} - \mathbf{X}_0) + \dot{\lambda}(\lambda - \lambda_0) - \Delta s$. Here, $\dot{\mathbf{x}}_0 = d\mathbf{X}/ds|_{\mathbf{X}=\mathbf{X}_0}$ and $\dot{\lambda} = d\lambda/ds|_{\lambda=\lambda_0}$ with $\|\dot{\mathbf{x}}_0\|^2 + |\dot{\lambda}|^2 = 1$. The extended system corresponds to finding a solution that lies on the plane perpendicular to $(\dot{\mathbf{x}}_0, \dot{\lambda}_0)$ that intersects the solution curve, which is shown graphically in Figure S1.

With access to the Jacobian of the system ($d\mathbf{F}/d\mathbf{X}$), one can obtain the tangent vector $(\dot{\mathbf{x}}_0, \dot{\lambda}_0)$ exactly (up to the sign of $\dot{\lambda}_0$). In this work, the Jacobian is not convenient to use. We approximate the tangent vector by taking initial natural continuation steps (5 usually) in λ using then switch to PAC by using approximating $(\dot{\mathbf{x}}_0, \dot{\lambda}_0)$ based on previous solution points. To solve for the next point, we take a predictor step to the point $(\mathbf{X}_0 + \dot{\mathbf{x}}_0\Delta s, \lambda_0 + \dot{\lambda}_0\Delta s)$ and use Anderson Acceleration to solve the extended system.

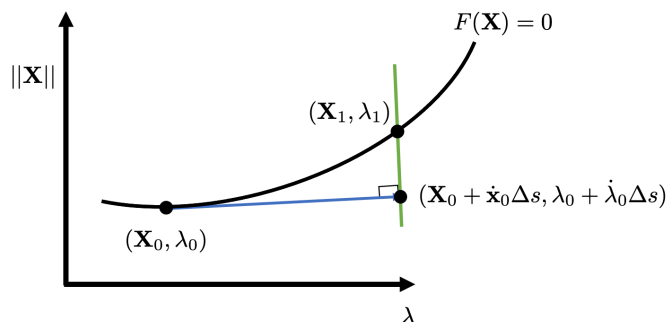


Figure S1: Graphical illustration of pseudo-arclength continuation. Continuation proceeds along the solution curve defined by $\mathbf{F}(\mathbf{X}) = 0$ from an initial point $(\mathbf{X}_0, \lambda_0)$ to $(\mathbf{X}_1, \lambda_1)$ by solving the extended system of equations $G = [\mathbf{F}(\mathbf{X}(s), \lambda(s)), N(\mathbf{X}(s), \lambda(s))]$.

S2 Thermodynamic Stability and Turning Points

Figure S2 shows a prototypical example of the adsorption isotherm and corresponding excess grand potential energy (equivalent to the surface tension). Each plot is divided into multiple colors that indicate the phase adjacent to the surface. The red lines indicate a thermodynamically unstable region. From thermodynamics of a single component system, thermodynamic stability requires that the 2nd derivative of the free energy with respect to chemical potential be negative.^{S8} This is true for a multicomponent system if the other chemical potentials are kept constant. In the adsorption process in Figure S2, the salt ion chemical potentials change along with the polyelectrolyte chemical potentials so rigorously, one cannot determine stability from Figure S2 alone. However, practically, for the conditions here, the change in the chemical potential of the salt ions is small. The 2nd derivative is clearly negative for the blue and black regions and positive for the red region of Figure S2b. Further, we can see from Figure S2b that there are regions of metastability. For example, there is a section where the free energy (surface tension) is higher for the supernatant phase,

yet a stable phase exists on the surface. The same is true for the coacervate layer. Finally, the crossing of the blue and black curves in Figure S2b is the coexistence point of the supernatant and coacervate phase on the surface.

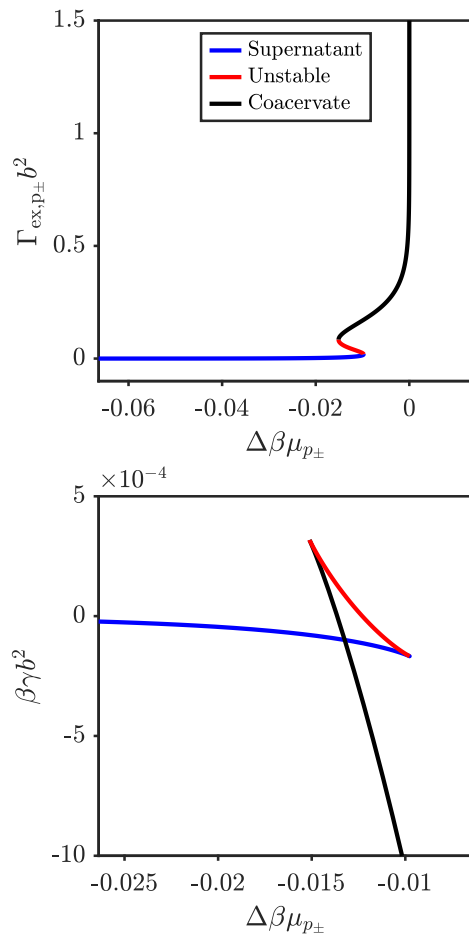


Figure S2: (a) Symmetric adsorption isotherm with $\beta\eta_{p_{\pm}} = -0.05$ for a constant overall salt fraction $\phi_{\pm}^{\text{B}} = 0.1$. (b) Corresponding surface tension (excess grand potential) for the adsorption isotherm in (a).

Figure S3 shows the surface free energy for one of the adsorption isotherms in Figure 2 of the main text. Namely, for $\beta\eta_{p_{\pm}} = -0.01$ and overall salt fraction $\phi_{\pm}^{\text{B}} = 0.1$, the system is below the wetting salt concentration so partial wetting takes place. With partial wetting, it's possible to have a metastable coacervate film on the surface with diverging film thickness, but the film does not cross the supernatant branch to be globally stable.

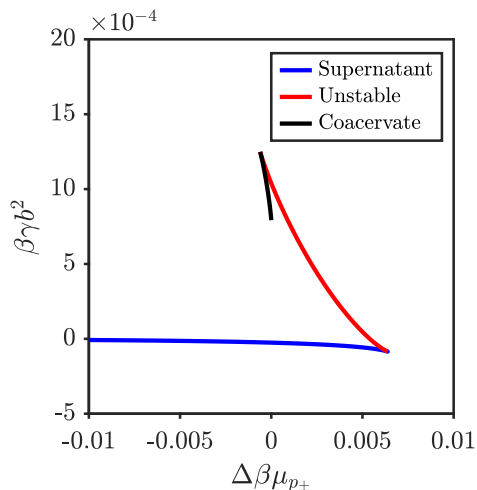


Figure S3: Surface tension corresponding to adsorption isotherm with $\beta\eta_{p\pm} = -0.01$ for a constant overall salt fraction $\phi_{\pm}^B = 0.1$.

S3 First to Second Order Surface Transition

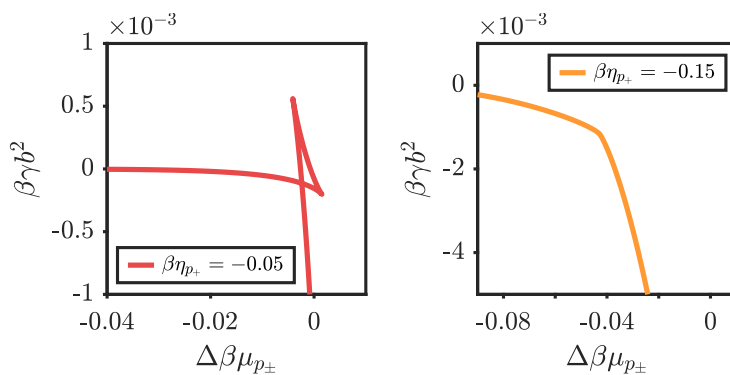


Figure S4: Surface tension (surface excess grand potential energy) for (a) $\beta\eta_{p+} = -0.05$ and (b) $\beta\eta_{p+} = -0.15$. $\Delta\mu_{p\pm} = \mu_{p\pm} - \mu_{p\pm}^{\text{coex}}$ is a measure of the distance from coexistence. Panel (a) shows the typical surface tension profile for a first order transition, featuring metastable and unstable regions. Panel (b) shows the typical surface tension profile for a second order transition, where the surface tension and first derivative of the surface tension transition smoothly from a supernatant to a coacervate surface phase. Corresponding adsorption isotherms can be found in Figure 4 of the main text.

S4 Symmetric Adsorption with Applied Potential

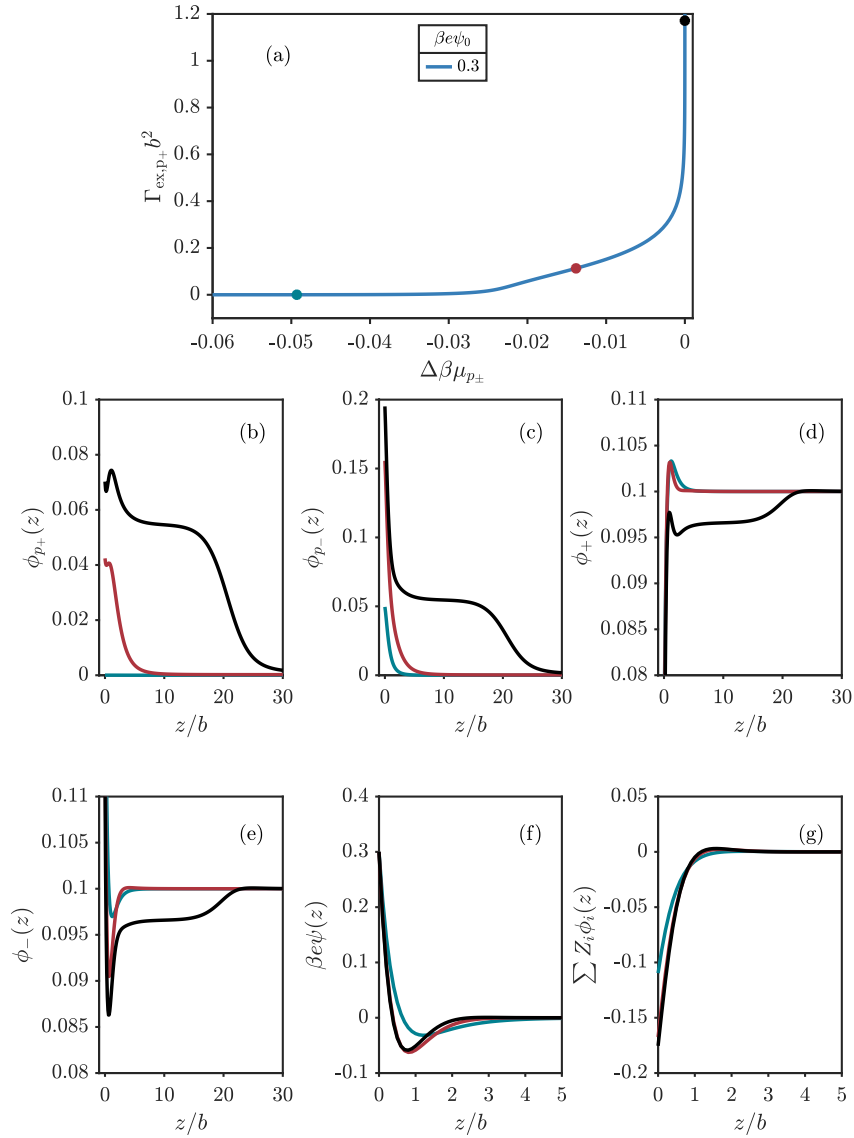


Figure S5: (a) Polyelectrolyte adsorption isotherms for $\beta e\psi_0 = 0.3$ at a constant bulk salt concentration of $\phi_{\pm}^B = 0.1$ with $\beta\eta_{p\pm} = -0.05$. Corresponding (b) polycation, (c) polyanion, (d) cation, (e) anion, (f) electrostatic potential, and (g) charge density for the solid points in (a). Notably, the surface potential and charge density cross zero in panels (f) and (g), respectively. Based on initially weak adsorption of polycation in (a) and strong adsorption of polyanion in (b) (green curves), we state in the main text that the wetting transition proceeds predominantly from the electrostatic attraction between adsorbed polyanion attracting polycation to the surface.

S5 Interfacial Tension in Contact Angle Calculation

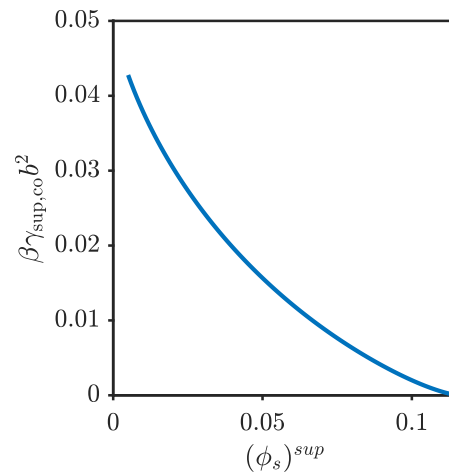


Figure S6: Interfacial tension of supernatant–coacervate phase versus the supernatant salt concentration calculated via the same method in Zhang and Wang.^{S9} The interfacial tension vanishes at the bulk critical point. The parameters in this figure correspond to that of the phase diagram in Figure 1 in the main text.

S6 Additional Prewetting Transition (Layering Transition)

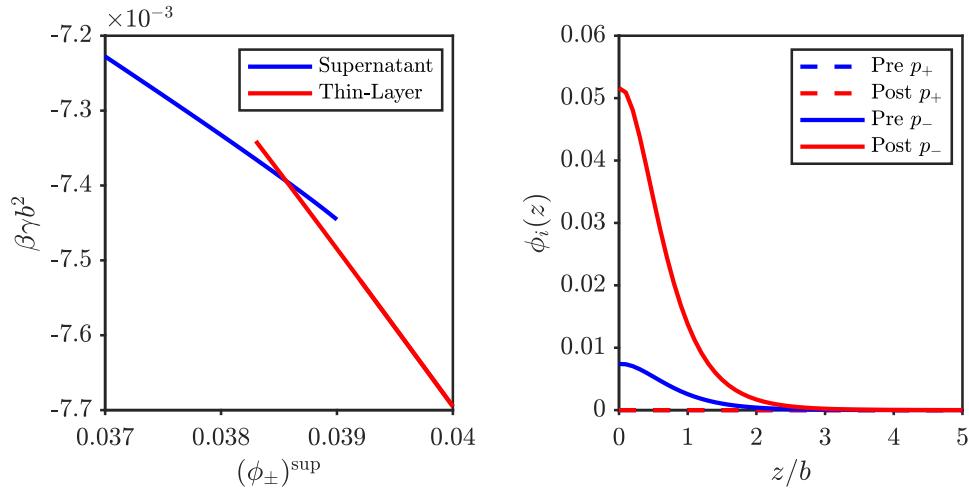


Figure S7: (left) Excess grand potential (surface tension) versus supernatant salt concentration for $\beta\eta_{p_{\pm}} = 0.01$ and $\beta e\psi_0 = 0.5$. (right) Interfacial profile for polycation (dashed) and polyanion (solid) before and after the prewetting transition, corresponding to $(\phi_{\pm})^{\text{sup}} = 0.038$ and $(\phi_{\pm})^{\text{sup}} = 0.039$, respectively. The before and after profiles overlap for the polycation, indicating the polyanion drives the transition. The wetting salt concentration for these conditions is $\phi_{\pm}^{\text{wet}} = 0.083$ so the transition occurs below the wetting salt concentration. A first order transition below the wetting salt concentration is an additional prewetting transition. Multiple prewetting transitions of the same kind are possible, which correspond to polyelectrolyte multi-layers forming on the surface.

S7 Effect of Polyelectrolyte Adsorption on Supernatant Surface Tension

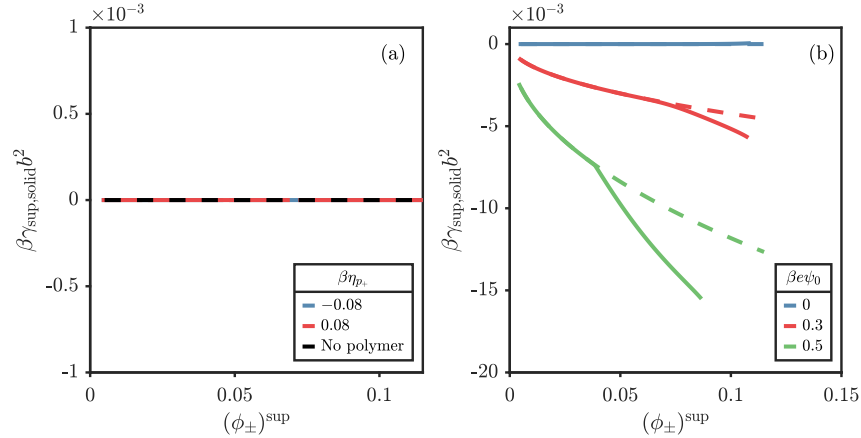


Figure S8: (a) Comparison of $\gamma_{\text{sup,solid}}$ for asymmetric nonelectrostatic adsorption ($\beta\eta_{p-} = 0$). Solid lines correspond to uniformly mixed description and dashed lines correspond to a polyelectrolyte-free solution at the same osmotic pressure as the coacervate phase. All lines overlap, which indicates that the polyelectrolyte adsorption (or desorption) does not appreciably affect the supernatant–solid surface tension. (b) Comparison of $\gamma_{\text{sup,solid}}$ for symmetric nonelectrostatic adsorption ($\beta\eta_{p\pm} = 0.01$) for different applied potentials. Solid lines correspond to uniformly mixed description and dashed lines correspond to a polyelectrolyte-free solution at the same osmotic pressure as the coacervate phase. The green and red lines show differing behavior between the uniformly mixed polyelectrolytes and polyelectrolyte-free cases, indicating the effect of polyelectrolyte adsorption on the supernatant–solid surface tension.

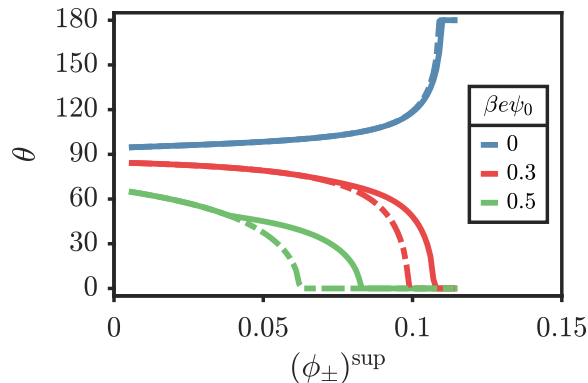


Figure S9: Contact angle versus the supernatant salt fraction when applying a surface potential for $\beta\eta_{\pm} = 0.01$. Critical salt concentration is $\phi_{\pm}^{\text{crit}} = 0.115$. The calculation of the contact angle uses the supernatant–solid surface tensions from Figure S8. Solid lines correspond to uniformly mixed description and dashed lines correspond to a polyelectrolyte-free solution at the same osmotic pressure as the coacervate phase. Again, the effect of the polyelectrolyte adsorption is enhanced as the applied potential increases in magnitude.

References

- (S1) Keller, H. B. *Numerical solution of bifurcation and nonlinear eigenvalue problems*; Academic Press: New York, 1977; pp 359–384.
- (S2) Salinger, A. G.; Burroughs, E. A.; Pawlowski, R. P.; Phipps, E. T.; Romero, L. A. Bifurcation tracking algorithms and software for large scale applications. *International Journal of Bifurcation and Chaos in Applied Sciences and Engineering* **2005**, *15*, 1015–1032, DOI: 10.1142/S0218127405012508.
- (S3) Nold, A.; Malijevský, A.; Kalliadasis, S. Wetting on a spherical wall: Influence of liquid-gas interfacial properties. *Physical Review E - Statistical, Nonlinear, and Soft Matter Physics* **2011**, *84*, 21603, DOI: 10.1103/PhysRevE.84.021603.
- (S4) Yatsyshin, P.; Savva, N.; Kalliadasis, S. Spectral methods for the equations of classical density-functional theory: Relaxation dynamics of microscopic films. *Journal of Chemical Physics* **2012**, *136*, 124113, DOI: 10.1063/1.3697471.
- (S5) Yatsyshin, P.; Savva, N.; Kalliadasis, S. Wetting of prototypical one- and two-

- dimensional systems: Thermodynamics and density functional theory. *Journal of Chemical Physics* **2015**, *142*, 34708, DOI: 10.1063/1.4905605.
- (S6) Lin, E. Y.; Frischknecht, A. L.; Winey, K. I.; Riggleman, R. A. Effect of surface properties and polymer chain length on polymer adsorption in solution. *Journal of Chemical Physics* **2021**, *155*, 034701, DOI: 10.1063/5.0052121.
- (S7) Chan, T. F. Newton-Like Pseudo-Arclength Methods for Computing Simple Turning Points. *SIAM Journal on Scientific and Statistical Computing* **1984**, *5*, 135–148, DOI: 10.1137/0905010.
- (S8) Callen, H. B. *Thermodynamics and an Introduction to Thermostatistics*, 2nd ed.; John Wiley & Sons, Inc., 1985; pp 203–276.
- (S9) Zhang, P.; Wang, Z.-G. Interfacial Structure and Tension of Polyelectrolyte Complex Coacervates. *Macromolecules* **2021**, *54*, 10994–11007, DOI: 10.1021/acs.macromol.1c01809.